applied sciences

MDPI

Article

Mapping Nanoparticles in Hydrogels: A Comparison of Preparation Methods for Electron Microscopy

Harald Ian Muri [1,*], Linh Hoang [2] and Dag Roar Hjelme [1]

[1] Department of Electronic Systems, Norwegian University of Science and Technology, O. S. Bragstads plass 2 B, 7034 Trondheim, Norway; dag.hjelme@ntnu.no

[2] Department of Clinical and Molecular Medicine/Cellular and Molecular Imaging Core Facility, Norwegian University of Science and Technology, 7491 Trondheim, Norway; linh.hoang@ntnu.no

* Correspondence: harald.muri@ntnu.no; Tel.: +47-7341-2688

Received: 30 October 2018; Accepted: 29 November 2018; Published: 1 December 2018

Abstract: The distribution of noble metal nanoparticles (NMNPs) in hydrogels influences their nanoplasmonic response and signals used for biosensor purposes. By controlling the particle distribution in NMNP-nanocomposite hydrogels, it is possible to obtain new nanoplasmonic features with new sensing modalities. Particle positions can be characterized by using volume-imaging methods such as the focused ion beam-scanning electron microscope (FIB-SEM) or the serial block-face scanning electron microscope (SBFSEM) techniques. The pore structures in hydrogels are contained by the water absorbed in the polymer network and may pose challenges for volume-imaging methods based on electron microscope techniques since the sample must be in a vacuum chamber. The structure of the hydrogels can be conserved by choosing appropriate preparation methods, which also depends on the composition of the hydrogel used. In this paper, we have prepared low-weight-percentage hydrogels, with and without gold nanorods (GNRs), for conventional scanning electron microscope (SEM) imaging by using critical point drying (CPD) and hexamethyldisilazane (HMDS) drying. The pore structures and the GNR positions in the hydrogel were characterized. The evaluation of the sample preparation techniques elucidate new aspects concerning the drying of hydrogels for SEM imaging. The results of identifying GNRs positioned in a hydrogel polymer network contribute to the development of mapping metal particle positions with volume imaging methods such as FIB-SEM or SBFSEM for studying nanoplasmonic properties of NMNP-nanocomposite hydrogels.

Keywords: metal nanocomposite hydrogels; particle positions; nanoplasmonic sensor; preparation methods; SEM imaging; volume imaging

1. Introduction

The ability of a hydrogel to absorb large amounts of water without being dissolved has shown to be useful in a significant number of applications, such as drug delivery systems, wound healing, protein purification, crystallization of minerals, distillation, pollutant capturing, and sensor technologies [1–10]. The hydrogel properties can be designed by controlling the crosslinking density, the polymer hydrophilicity, the type of recognition entities, polymer ionicity, or polymer elasticity. The common functions of the polymer network consist of responding volumetrically to external stimuli such as pH [11–13], temperature [14–17], ionic strength [18–20], or receptor–analyte recombinations [21–24]. Some of these stimuli-responsive features have shown to be very useful in controlling drug release [1] or to be useful for label-free and specific sensing of biomolecules [22,25]. By filling the hydrogel with composite materials such as polymeric fibers, carbon-based or metal nanostructures, and amorphous or crystalline inorganic materials, the stability of stimuli-responsive

hydrogels as well as its homogeneity can be enhanced, and new functionalities can be added in terms of sensor selectivity, sensor specificity, and new sensor techniques [26–29]. These nanocomposite hydrogels with noble metal nanoparticles (NMNPs) are fascinating materials, often utilized for wound healing [30,31], but are also impressive materials as nanoplasmonic systems [32,33]. In membrane technology, NMNPs have also shown to be a potential candidate for development in thermoplasmonics that may improve nanofiltration, pervaporation processes, or oil-in-water nanoemulsions [34–37]. Hydrogels with NMNPs as composite materials exhibit intense optical scattering at specific light frequencies. These phenomena arise from light interacting with confined collective oscillations of electron clouds in the NMNPs at a resonance frequency, also known as localized surface plasmon resonance (LSPR) [38–40]. The LSPR of NMNPs may occur in the visible or infrared light-range and are frequently used in label-free biosensor applications due to fast response times, high sensitivity, high selectivity, and the possibility for multianalyte sensing in complex mixtures [38,41–44]. The LSPR of NMNP-nanocomposite hydrogels are dependent on the particle shape, the size, the refractive index (RI) of the surrounding medium, and the interparticle distances [44,45]. Coupling may occur between the resonant modes of the localized surface plasmons of NMNPs in close proximity to each other [44,46–49]. The scattering of NMNPs in a hydrogel may have an LSPR frequency for a random distribution of particles that is different from the LSPR frequency for an inhomogeneous particle distribution.

We have in earlier work developed proof-of-concepts of fiber optic (FO) sensors based on using NMNPs immobilized in polyacrylamide hydrogels and combining LSPR and interferometric sensing modalities [25,50–53]. The interferometric sensing modality detects the change in volume of a stimuli-responsive hydrogel, whereas the LSPR sensing modality detects receptor–analyte recombinations on the NMNP surface. The dipole–dipole coupling and RI sensitivity of the LSPR in NMNPs may as well be utilized for detecting the change in volume of stimuli-responsive hydrogels for significant swelling and deswelling. The LSPR response of spherical or spheroidal gold nanoparticles (GNP) in hydrogels has shown to deviate from the LSPR response of randomly distributed spherical or spheroidal GNPs [51–53]. The plasmon coupling between spherical GNPs occurred for an interparticle distance that was larger than the estimated plasmon coupling distance [51]. This was found to be due to the inhomogeneous distribution of the particles in the hydrogel. The LSPR response for decreasing interparticle distances, where dominated by the side-by-side plasmon coupling between spheroidal GNPs [53]. This was likely due to an ordered tendency of the spheroidal particles in the hydrogel. To further understand and engineer the LSPR properties of GNP-nanocomposite hydrogels for biosensing purposes, it is desirable to identify how the particles are ordered and distributed from morphological characterizations.

Morphological characterizations of hydrogels are often performed by using scanning electron microscopy (SEM). By using specialized microscopy techniques, such as cryoSEM, environmental-SEM, or time-of-flight secondary ion mass spectrometry (TOF-SIMS), it is possible to characterize the morphology of hydrogels in their swelled state [54–56]. However, specialized microscopy techniques may have limited accessibility due to being a state-of-the-art technology that increases the user costs. Conventional SEM techniques require the samples to be in a vacuum, which can pose challenges for conserving the native hydrated state of the hydrogel since its structure is contained by the water absorbed in the polymer network. To prevent a complete collapse of the hydrogel in the SEM vacuum chamber, one can use drying methods such as high or low temperature drying [17,57–59] or critical point drying (CPD) [55,58,60,61] to conserve its pore structure. Different collapsing characteristics occur depending on the drying methods used and the composition of the hydrogel [58,62,63]. By using transmission electron microscopy (TEM), the high contrast of metal nanoparticles embedded in hydrogels can be observed; however, only a two-dimensional particle positions can be quantized [64,65]. To map the three-dimensional positions of particles in hydrogels with volume imaging methods, such as the focused ion beam-SEM technique (FIB-SEM) [66–68], conventional drying methods must be used. The CPD technique is a common method for drying hydrogels or biological materials to

conserve the morphology in SEM imaging [55,58,60,61]. An alternative to CPD is to dry the samples with hexamethyldisilazane (HMDS) solvent in air. The surface tension of the sample is reduced by using HMDS, and it may also cross-link proteins for biological materials [69]. This is adding strength to the sample during air-drying and prevents collapse or fracturing. A comparison of samples dried with CPD or HMDS for SEM have in previous work often been performed for biological specimens [70–73]. The air-drying with HMDS as an alternative to the CPD technique has its advantages: (1) less effort and fewer variables are involved; (2) it is cost-effective; and (3) the method requires no equipment use such as for controlling carbon dioxide phase changes. The HMDS may reduce surface tension for all hydrophilic materials and, therefore, serve as a useful drying method for hydrogels. The HMDS drying of fibrin or elastin hydrogels have been described in earlier work [74–77]. Additionally, the sputter coating of the sample may have to be optimized concerning coating thickness and coating material. Samples with significant differences in the topography may require a thicker coating than for samples with small differences in topography; i.e., the SEM imaging of the GNPs and the hydrogel structure may have conflicting requirements. The optimization of the sputter coating is beyond the scope of this article. Furthermore, since swelling and molecular transport properties of acrylamide hydrogels have been discussed in earlier work [25,50], the characterization of mechanical and rheological properties have not been included.

Here, the morphology of 10 wt % polyacrylamide (AAM-BIS) and poly(acrylamide-co-acrylic acid) (AAM-AAC-BIS) hydrogels, with and without gold nanorods (GNRs) as composite materials, was studied using conventional SEM. Low GNR densities were used ($10/\mu m^3$) as for the earlier FO sensor studies in [51–53]. The hydrogels were prepared for SEM using CPD or the drying with HMDS and characterized concerning pore structures and GNR positions in the polymer network. Pore sizes were estimated and compared for hydrogels with and without GNPs as well as compared for CPD hydrogels and HMDS-dried hydrogels. The evaluation of the sample preparation methods may confirm or introduce new aspects of hydrogel drying techniques with respect to the limited literature available in this field. The results concerning the identification of GNRs positioned in hydrogel polymer network may serve as a contribution to the development of mapping particle positions in hydrogels by using volume imaging methods, such as the FIB-SEM or the serial block-face scanning electron microscopy (SBFSEM) techniques [66–68,78,79]. By identifying how the particles are ordered and positioned in NMNP-nanocomposite hydrogels, LSPR properties can be defined and further engineered.

2. Experimental Section

2.1. Materials for Synthesizing Hydrogels

The materials used for synthesizing hydrogels, with and without GNPs, are as follows: acrylamide (AAM) (99%, Sigma Aldrich, Schnelldorf, Germany), acrylic acid (AAC) (99%, Sigma Aldrich, Schnelldorf, Germany), *N*,*N*-methylenebisacrylamide (BIS) (≥99.5%, Sigma Aldrich, Schnelldorf, Germany), 1-hydroxycyclohexyl phenyl ketone (99%, Sigma Aldrich, Schnelldorf, Germany), dimethyl sulfoxide (DMSO) (≥99.9%, Sigma Aldrich, Schnelldorf, Germany), citrate-stabilized 670 nm-resonant GNRs (50 nm in length, 19 nm in diameter, 1.14×10^{13} particles/mL, 2 mM citrate buffer, nanoCompix, San Diego, CA, USA), phosphate-buffered saline (PBS) (Tablet, Sigma Aldrich, Schnelldorf, Germany), squalane (99%, Sigma Aldrich, Schnelldorf, Germany), milli-Q (mQ) water (resistivity 18.2 MΩ/cm, Millipore Simplicity 185, Millipore Ltd., Toronto, ON, Canada), and pentane (Van Water & Rogers, VWR, Radnor, PA, USA).

2.2. Synthesizing Bulk Volume of Hydrogel With and Without Gold Nanoparticles

Two stock solutions were prepared and used later for making pre-gel samples. The first stock solution was prepared by dissolving AAM and BIS in PBS solution (30 wt % AAM-BIS and 2 mol % BIS). The second stock solution was prepared by dissolving AAM, AAC, and BIS in PBS solution (30 wt

% AAM-AAC-BIS, 2 mol % BIS, molar ratio AAM/AAC = 1/2). The stock solutions were stored at 4 °C until further use for up to two weeks. Pre-gel samples (10 wt % AAM-BIS and 10 wt % AAM-AAC-BIS) were further prepared by diluting the stock solutions with PBS or GNP solution. Four types of pre-gel samples were made: (1) 10 wt % AAM-BIS in PBS solution; (2) 10 wt % AAM-BIS in GNP solution; (3) 10 wt % AAM-AAC-BIS in PBS solution; (4) 10 wt % AAM-AAC-BIS in GNP solution. The pre-gel samples were stored at 4 °C until further use for up to 24 h. Next, 1-hydroxycyclohexyl phenyl ketone photoinitiator (PI) was diluted in DMSO (0.01 M). Before photopolymerization, the PI-DMSO solution was added to the pre-gel sample (with ratio PI/pre-gel = 31/2000). Pre-gel (0.2 mL) with PI solution was further transferred by a pipette (Finpippette F2, Thermo Scientific, VWR, Waltham, MA, USA) to a glass rod surrounded by 1.3 mL of squalane-PI oil (2.7 mg/mL PI) in a 1.5 mL Eppendorf tube (211-2164, VWR, Eppendorf, Hamburg, Germany). The deposited pre-gel with PI solution on glass rod forms a hemispherical shape since it is immiscible in the squalane-PI oil. The hemispherical pre-gel with PI on the glass rod was illuminated with light at 365 nm by using an Ø400 µm multimode OF (QP400-2-UV-VIS, Ocean Optics, Dunedin, FL, USA) connected to a LED (M365F1, Thorlabs, Newton, NJ, USA). The pre-gel with PI was photopolymerized for 15 min, subsequently transferred to pentane to remove impurities for 5 s and stored in PBS solution (pH of PBS adjusted to 4.5 for AAM-AAC-BIS hydrogel) until further use.

2.3. Preparing Hydrogels for Scanning Electron Microscopy

The materials used for preparing hydrogels for SEM are as follows: 2.5% glutaraldehyde (Chemi-Teknik AS, Oslo, Norway) in Sorensen's phosphate buffer (SPBS, VWR, Hatfield, PA 19440, USA) (pH 7.2), ethanol (absolute alcohol, Antibac AS, Oslo, Norway), and hexamethyldisilazane (HMDS) (≥99%, Sigma-Aldrich, Schnelldorf, Germany).

The AAM-BIS and AAM-AAC-BIS hydrogels, with and without GNP, were fixated in 2.5% glutaraldehyde (Chemi-Teknik AS, Oslo, Norway) in SPBS (pH 7.2) for 2 h at room temperature and left for 12 h at 4 °C. After fixation, the hydrogels were washed twice for 5 min in SPBS. The pre-gel samples were further cut in half by a razor, where one half was prepared for the critical point drying technique (CPD) (Polaron, Quorum Technologies Ltd., East Sussex, UK) and the other half was prepared for drying using an HMDS solvent. Before drying, the hydrogels were dehydrated with increased ethanol concentrations of 10, 25, 50, 70, 90, and 100%, 5 min for each concentration. Further, one gel serie from the razor cutting was transferred to the CPD, while the other gel serie was transferred to the HMDS solvent. With the CPD technique, the ethanol was replaced with liquid carbon dioxide and sublimed entirely. With the HMDS solvent, the gel was transferred to 50% HMDS diluted in ethanol for 20 min and transferred to a new 50% HMDS in ethanol solution for another 20 min. Next, the gel was transferred to 100% HMDS for 20 min and transferred to a new 100% HMDS solution. The hydrogels in the HMDS solvent were then dried overnight in a desiccator. The dried samples were cracked in two by a razor, mounted on pins using double-sided carbon tape, and sputter-coated (E5100, Polaron, Quorum Technologies Ltd., East Sussex, UK) with 30 nm of gold–palladium (Au/Pd). The samples were examined using a scanning electron microscope (Teneo Volumescope, Thermo Scientific Fisher, Waltham, MA, USA), using an Everhart–Thornley detector (ETD) in secondary electron (SE) mode and Trinity detector (T1) in backscattered electron (BSE) mode. ImageJ (NIH) was used for morphology analysis. The mean and standard deviation of the Feret diameters of the pore sizes in the hydrogel were calculated by applying threshold filters and particle analyzing functions on the SEM images.

2.4. Preparing GNPs on Carbon Tape for Scanning Electron Microscopy

An aliquot of GNP solution was transferred to double-sided carbon tape, dried overnight in a desiccator, and sputter-coated with 30 nm gold–palladium (Au/Pd). This prepared sample does not serve as a control for the experiments but are used as a comparison for how an image with GNRs can appear in an SEM image.

2.5. Sample Preparation and Imaging Technique Limitations

The comparison of sample preparation methods may only be limited to the hydrogel drying with CPD and HMDS since the methods are often developed for reducing the surface tension in biological materials. The results obtained may not be compared to other drying methods such as high or low temperature drying. Furthermore, the rehydration of hydrogels in humid or liquid environments after drying may complicate cross-sectional sample preparations. After fixation, hydrogels can be embedded and dried in materials such as epoxy polymers for cross-sectional analysis using ultramicrotomy with TEM or SEM. The ultramicrotomy is often performed in water and may therefore reduce the stability of the hydrogel structure due to rehydration. Thus, the sample preparations may only be restrained to cross-sectional sample preparations in dry environments, e.g., when utilizing ion-milling. Due to challenges in obtaining even surfaces from cross-sectional sample preparations, the use of scanning probe microscopy techniques have been omitted in this paper.

Since specialized microscopy techniques such as cryo-SEM, environmental-SEM, or TOF-SIMS may have limited accessibility that increases user costs, it is more feasible to focus on conventional electron microscopy and sample preparation techniques that are often used for biological samples such as eukaryotic and prokaryotic cells. Hence, the imaging technique used is restrained to electron microscopy with vacuum chambers and by detecting SE and BSE. By focusing on detecting mainly SE and BSE intensities, the studies are limited by assuming that the GNRs are embedded in the hydrogel after fixation, dehydration, and drying. This assumption is based on previous results obtained in different hydrogel-GNR sensor configurations in [51–53], where the LSPR signal was stable during different swelling experiments, i.e., the GNRs were shown to be contained in the hydrogel. Due to these results, the use of general distribution analytical techniques such as X-ray photoelectron spectroscopy (XPS), energy-dispersive X-ray spectroscopy (EDAX), or prompt gamma neutron activation analysis (PGAA) are omitted to direct the focus on morphological characterization and the study of GNRs positioned in hydrogel polymer networks.

3. Results and Discussion

3.1. Morphology of AAM-BIS Hydrogel With and Without GNRs

SEM images from CPD and HMDS-dried hydrogels with and without GNRs in SE and BSE mode are shown in Figure 1. Figure 1A,B show hydrogels prepared with CPD, while Figure 1C,D show HMDS-dried hydrogels. The mean and standard deviation of the Feret diameter of the pore sizes for the CPD hydrogels are 0.1405 ± 0.1006 μm and 0.2236 ± 0.1942 μm for the hydrogel without and with GNRs, respectively. The corresponding mean and standard deviation of the Feret diameter of the pore sizes for the HMDS-dried hydrogels are 0.1750 ± 0.1320 μm and 0.1421 ± 0.1156 μm for the hydrogel without and with GNRs, respectively. Thus, the pore sizes of the HMDS-dried and the CPD hydrogels are comparable, illustrating that using HMDS for drying hydrogels for SEM imaging may serve as a suitable alternative to the CPD technique. Furthermore, the mean pore size changes of $-0.03/+0.08$ μm when embedding GNRs in the hydrogel indicates that GNRs have a minor influence on the polymer network structure.

We expected to observe high-density materials, such as NMNPs, as high contrast segments in BSE mode at high electron beam voltages, since high-density materials have more substantial electron-backscattering intensities than low-density materials. However, the observed contrast features are similar for hydrogel with and without GNRs, which makes the quantizing of the position of GNRs in the polymer network uncertain. The small-sized contrast features shown with white arrows in Figure 1D could be characterized as GNR positions but may also be difficult to distinguish from artifacts associated with the sample preparation [80,81]. Without any immobilization, one might suspect that the GNRs will leak out of the hydrogel. However, results from our earlier study of LSPR of gold nanospheres embedded in AAM-BIS hydrogels were consistent with a uniform and stable particle distribution in the hydrogel volume [52]. These results show that the LSPR signal was stable over time

and for different swelling equilibriums. That the Feret diameters of the pore sizes of the AAM-BIS hydrogel are on the order of 200 nm suggests that the GNRs are bound to the polymer network of the hydrogel.

Figure 2 shows SEM images of CPD and HMDS-dried hydrogels with GNRs at higher magnification than in Figure 1. The SEM image of GNR solution dried on carbon tape in Figure 2B is included to enable direct comparison of how GNRs can appear in an SEM image. The small-sized contrast features in Figure 2B have lengths and widths similar to the GNR specifications received from the producer.

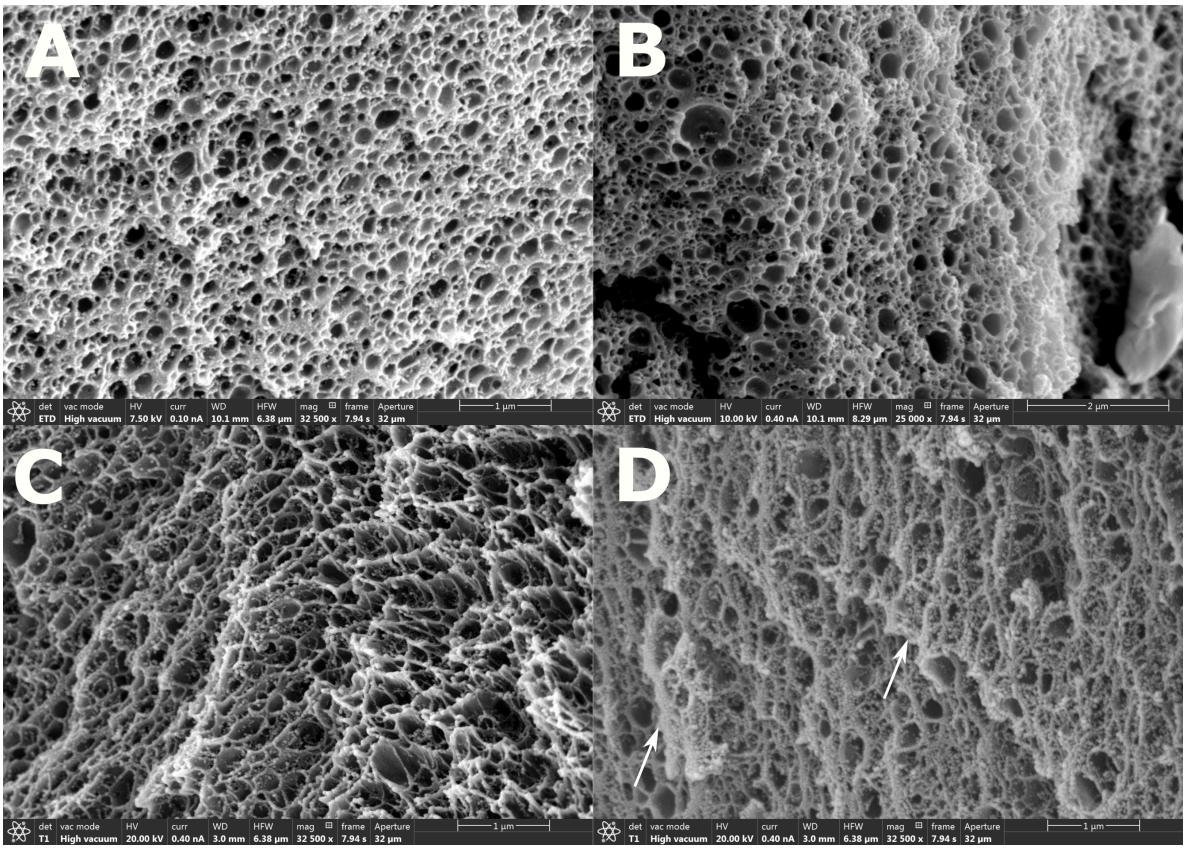

Figure 1. (**A**) Scanning electron microscope (SEM) image of critical point dried (CPD) AAM-BIS hydrogel without gold nanorods (GNRs) in SE mode; (**B**) SEM image of CPD AAM-BIS hydrogel with GNRs in SE mode; (**C**) SEM image of hexamethyldisilazane-dried (HMDS-dried) AAM-BIS hydrogel without GNP in backscattered electron (BSE) mode; (**D**) SEM image of HMDS-dried AAM-BIS hydrogel with GNP in BSE mode. Note that the scalebar in (**B**) is different from the other images. The white arrows show the small-sized contrast features observed that could indicate GNR positions.

The BSE mode SEM image shows few small-sized contrast features with dimensions comparable to the contrast features in Figure 2B, indicating the presence of GNRs. However, we did not succeed in pinpointing the contrast segments indicating particles using threshold filters on the images. The contrast differences in the SEM images indicating GNPs cannot be proved without additional measurements. This is in accordance with the observation in [82], where cryoSEM was used for characterizing GNPs in polyacrylamide hydrogels. The contrast of NMNPs in gel-like samples may be improved by omitting the metal sample coating and by including highly conductive sample holders instead [83]. The detection of SE and BSE can also be combined to obtain density-dependent contrasts that highlights the high densities areas in the image [84].

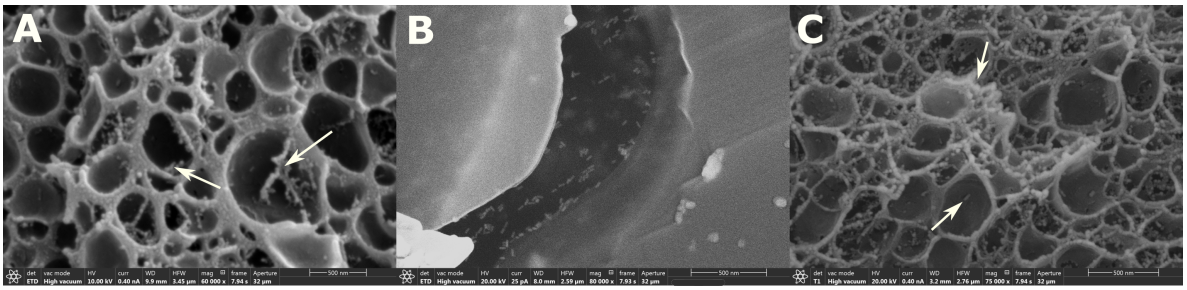

Figure 2. (**A**) SEM image of CPD AAM-BIS hydrogel with GNRs in SE mode; (**B**) air-dried GNR solution on carbon tape in SE mode for comparison with SEM images of GNP-hydrogels; (**C**) SEM image of HMDS-dried AAM-BIS hydrogel with GNP in BSE mode. The white arrows show the small-sized contrast features observed that could indicate GNR positions.

3.2. Morphology of AAM-AAC-BIS Hydrogel With and Without GNRs

SEM images of CPD and HMDS-dried hydrogels, with and without GNRs, in SE and BSE mode are shown in Figure 3.

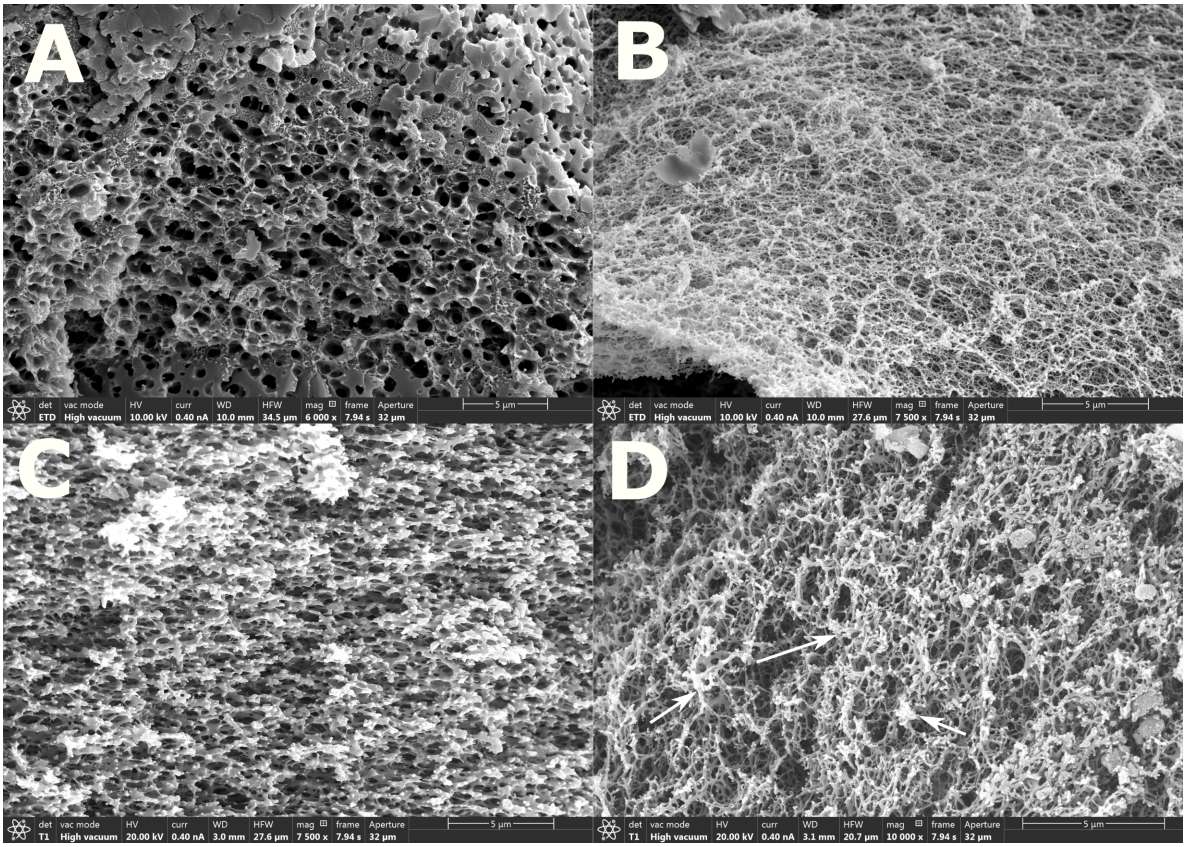

Figure 3. (**A**) SEM image of CPD AAM-AAC-BIS hydrogel without GNRs in SE mode; (**B**) SEM image of CPD AAM-AAC-BIS hydrogel with GNRs in SE mode; (**C**) SEM image of HMDS-dried AAM-AAC-BIS hydrogel without GNP in BSE mode; (**D**) SEM image of HMDS-dried AAM-AAC-BIS hydrogel with GNP in BSE mode. Note that the scalebar in the images is 5 µm. The white arrows show the small-sized contrast features observed that could indicate GNR positions.

Figure 3A,B show CPD hydrogels in SE mode, while Figure 3C,D show HMDS-dried hydrogels in BSE mode. The mean and standard deviation of the Feret diameter of the pore sizes for the CPD hydrogels are 0.6240 ± 0.4775 µm and 0.1219 ± 0.1050 µm for the hydrogel without and with GNRs, respectively. The corresponding mean and standard deviation of the Feret diameter of the pore sizes for the HMDS-dried hydrogels are 0.4190 ± 0.3570 µm and 0.0932 ± 0.0908 µm for the

hydrogel without and with GNRs, respectively. The significant increase in Feret diameter for hydrogel without GNRs may indicate a hydrogel collapse where many smaller pores have merged into larger pores. The collapse could be a result of insufficient dehydration considering that the AAM-AAC-BIS hydrogels have 2/1 (AAC/AAM) molar ratio of hydrophilic anionic AAC co-monomers. For CPD, the hydrogels may have been rehydrated due to the humidity at room temperature while transferring it to the CPD. Ethanol will only exchange efficiently with liquid carbon dioxide, so a partly rehydrated hydrogel will be more susceptible to a collapse. For HMDS drying, the hydrogel may have been rehydrated, while substituting ethanol with HMDS. HMDS may also only exchange efficiently with ethanol. This suggests that the HMDS-dried hydrogel is also susceptible to collapse due to rehydration. For hydrogels with GNRs, the Feret diameter is significantly smaller. This may indicate that the GNR-hydrogel has been less susceptible to a collapse.

The Feret diameters for the AAM-AAC-BIS GNR-hydrogels are also smaller than the AAM-BIS hydrogels in Section 3.1. This could be due to the hydrophilicity of the AAM-AAC-BIS hydrogels. The anionic AAC co-monomer may contribute to the absorption of a more substantial fraction of water into small pores of the polymer network in its original state. The preparation methods may also influence the pore structures as discussed in Section 3.3 [57,58].

As for the results obtained in Section 3.1, there are high contrast features along the edges of the polymer networks in Figure 3D in BSE mode (indicated by white arrows), which could represent dense materials. However, the contrast features are similar for hydrogel, with and without GNRs, and make the quantizing of the positions of GNRs in the polymer network uncertain. The sizes and shapes of the contrast features could be a result of the artifacts introduced from the sample preparations [80,81]. The studies of LSPR of GNPs in AAM-AAC-BIS hydrogels have been discussed in [51,53]. The LSPR signal did not decay for different hydrogel swelling equilibriums and indicated that the GNPs were contained in the hydrogel. Since the Feret diameters of AAM-AAC-BIS hydrogels with and without GNRs are in the order of 90 to 600 nm, it may be that the gold rods are bound to the polymer network of the hydrogel.

Figure 4 shows SEM images of CPD and HMDS-dried hydrogels with GNRs at a higher magnification than the SEM images in Figure 3.

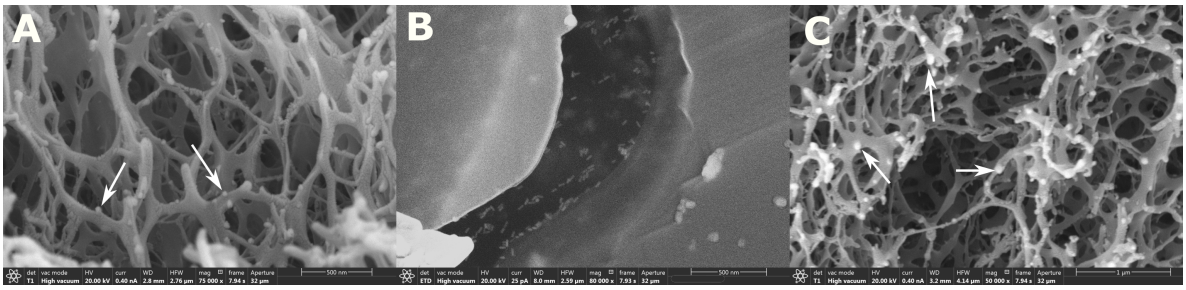

Figure 4. (**A**) SEM image of CPD AAM-AAC-BIS hydrogel with GNRs in BSE mode; (**B**) air-dried GNR solution on carbon tape in SE mode for comparison with SEM images of GNP-hydrogels; (**C**) SEM image of HMDS-dried AAM-AAC-BIS hydrogel with GNP in BSE mode. Note that the scalebar in (**C**) is different from the other images. The white arrows shows the small-sized contrast features observed that could indicate GNR positions.

The SEM image of GNR solution dried on carbon tape in Figure 4B is presented for comparison with the small-sized contrast features observable in Figure 4A,C shown with white arrows. In Figure 4A,C, the polymer network has a branched structure as compared to the AAM-BIS hydrogels. The branched polymer structure could be due to the hydrophilic nature of the anionic polymer network as discussed for Figure 3, where the Feret diameter was smaller than AAM-BIS GNR hydrogels. The small contrast features in Figure 4A,C (shown with white arrows) are similar to those in Figure 2A,C, which could indicate the presence of GNRs since they are denser than the polymer network. As discussed for the results in Figure 2, these contrast features are difficult

to quantize as GNR positions but could be improved by using results from [83,84]. Additionally, for the SEM images of AAM-AAC-BIS-GNR hydrogels, it was not feasible to identify GNRs by using threshold filters. Results obtained from work in [85] used conventional SEM to characterize poly(N-isopropylacrylamide)-co-(acrylic acid) microgels with GNPs and can be used for comparison. In this paper, EDAX was used for confirming the general distribution of GNPs. However, TEM had to be utilized to study the particle positions in the hydrogel.

3.3. Influence of Fixation, Dehydration, and Drying on the Morphological Structures of the GNR-Hydrogel

The AAM-BIS hydrogel is sensitive towards ethanol concentrations, but insensitive to pH for the solutions used in this paper [86]. The fixation with glutaraldehyde at pH 7.2 will, therefore, introduce small changes in the hydrogel swelling equilibrium with respect to changes in pore size and shapes. For the dehydration with ethanol, the hydrogel will decrease in size, which can be assumed to result in considerable changes in the size and shape of pores of the polymer network. The pore sizes observed in Figures 1 and 2 are, therefore, likely to be smaller than the pore size of the hydrogel in a hydrated state. The dried hydrogels may also in most cases exhibit an uncertain degree of collapsing characteristics [57,58,62,63,87]. Any degree of collapsing characteristics of the hydrogel may result in a close packing of the GNRs. The amount of close-packed GNRs in the BSE mode SEM images were difficult to characterize in our results due to the low contrast of GNRs. Other microscopy techniques may be used to study its native hydrated state such as by using cryogenic or environmental SEM that omits the fixation, dehydration, and drying [54,55].

The AAM-AAC-BIS hydrogel is sensitive to both ethanol and pH [86,88]. The fixation with glutaraldehyde at pH 7.2 causes the hydrogel to swell significantly due to the deprotonation of the AAC, making the polymer network highly anionic. This may pose a strain on the polymer network beyond the elastic limit. Thus, the branched polymer network in Figure 3B,D could be a result of the swelling of the hydrogel. The dehydration of the hydrogel with ethanol causes the hydrogel to contract significantly. The pore size observed in Figures 3 and 4 is assumed to be smaller than the pore size of the hydrogel in its native hydrated state.

3.4. Summary of Results—Pore Structures

Results in Sections 3.1 and 3.2 are shown in Table 1 to present an overview of the computed mean and standard deviation of the Feret diameters in μm of the hydrogel pore structures.

Table 1. Mean and standard deviation of Feret diameters of hydrogel pore structures in μm. CPD: Critical Point Drying. HMDS: Hexamethyldisilazane.

Hydrogels / Drying Method	AAM-BIS	AAM-BIS-GNR	AAM-AAC-BIS	AAM-AAC-BIS-GNR
CPD	0.1405 ± 0.1006	0.2236 ± 0.1942	0.6240 ± 0.4775	0.1219 ± 0.1050
HMDS	0.1750 ± 0.1320	0.1421 ± 0.1156	0.4190 ± 0.3570	0.0932 ± 0.0908

4. Conclusions

The morphology of low-weight-percentage polyacrylamide and poly(acrylamide-co-acrylic acid) hydrogels, with and without GNRs, has been characterized using conventional SEM. A comparison was made between the CPD and HMDS drying methods of hydrogels with and without GNRs. Results of CPD and HMDS techniques show comparable pore structures, estimated by computing the mean Feret diameter in ImageJ. For acrylamide gels, the pore sizes were also comparable with and without GNRs. The use of an HMDS solvent for drying may serve as a suitable alternative to the CPD technique. The HMDS technique is a cost-effective substitution of the CPD technique that omits equipment use as well as being less time consuming. The poly(acrylamide-co-acrylic

acid) hydrogels have slightly smaller pores sizes than polyacrylamide hydrogels with branched polymer structure. This difference can be assumed to be due to the more substantial hydrophilicity of poly(acrylamide-co-acrylic acid) anionic hydrogel. The pore structures of the dehydrated and dried hydrogels are likely smaller than the pore structures of hydrated hydrogels due to the water exchange with ethanol in the dehydration. The dehydration and drying of hydrogels may result in an uncertain degree of collapsing characteristics [57,58,62,63,87]. By comparing the morphology of dried hydrogels with cryoSEM or environmental SEM images of hydrated hydrogels [54,55], it is possible to estimate the presence of these collapsing features.

Small-sized contrast elements can be observed from the BSE-mode SEM images of GNR-nanocomposite hydrogels and may indicate the presence of GNRs since they are denser than the polymer network. The contrast of these segments was not significant enough to distinguish them from artifacts associated with the sample preparations [80,81]. These results are consistent with similar studies in [82,85]. Additionally, the identification of GNRs with threshold filters was not feasible due to the small contrast differences. The contrast of NMNPs in gel-like samples may be improved by omitting the sample coating and by including highly conductive sample holders instead [83], or by using both SE and BSE detectors to obtain density-dependent contrasts that highlights the high densities areas in the image [84].

Further work is needed to increase the contrast of the metal particles in the polymer matrix so that a mapping of the GNP positions in hydrogels can be determined. However, an evaluation of preparation methods may elucidate new aspects concerning hydrogel drying techniques and GNR identification in the hydrogel polymer network. Since the pore sizes were comparable for acrylamide hydrogels with and without GNRs, it may also be that the hydrogel structure was nearly unaffected by adding GNPs to its matrix. Future work will consist of developing methods for enhancing the contrast of high-density materials in a low-density matrix for conventional SEM imaging. Furthermore, volume-imaging methods such as the FIB-SEM or the SBFSEM techniques will be used to map the positions of metal particles in nanocomposite hydrogels.

Author Contributions: H.I.M., L.H., and D.R.H. conceived and designed the experiments; H.I.M. and L.H. performed the experiments; H.I.M., L.H., and D.R.H. analyzed the data; H.I.M., L.H., and D.R.H. wrote the paper.

Funding: This work was supported by strategic research funding from Norwegian University of Science and Technology (NTNU). The work was also supported by the Interreg Sweden-Norway program (IR2015.01) and Energy and Sensor Systems (ENERSENSE, strategic research program at NTNU). The electron microscopy experiments were conducted in the EM laboratory at the Cellular and Molecular Imaging Core Facility (CMIC), NTNU.

Conflicts of Interest: The authors declare no conflict of interest.

References

1. Hoare, T.R.; Kohane, D.S. Hydrogels in drug delivery: Progress and challenges. *Polymer* **2008**, *48*, 1993–2007. [CrossRef]
2. Ratner, B.; Hoffman, A. Synthetic Hydrogels for Biomedical Applications. In *Hydrogels for Medical and Related Applications*; Andrade, J.D., Ed.; American Chemical Society: Washington, DC, USA, 1976; Volume 31, p. 1.
3. Caló, E.; Khutoryanskiy, V.V. Biomedical applications of hydrogels: A review of patents and commercial products. *Eur. Polym. J.* **2015**, *65*, 252–267. [CrossRef]
4. Xie, M.; Olderøy, M.Ø.; Andreassen, J.P.; Selbach, S.M.; Strand, B.L.; Sikorski, P. Alginate-controlled formation of nanoscale calcium carbonate and hydroxyapatite mineral phase within hydrogel networks. *Acta Biomater.* **2010**, *6*, 3665–3675. [CrossRef] [PubMed]
5. Gawel, K.; Barriet, D.; Sletmoen, M.; Stokke, B.T. Responsive Hydrogels for Label-Free signal transduction within biosensors. *Sensors* **2010**, *10*, 4381–4409. [CrossRef] [PubMed]
6. Lee, K.Y.; Mooney, D.J. Hydrogels for Tissue Engineering. *Chem. Rev.* **2001**, *101*, 1869–1880. [CrossRef] [PubMed]
7. Holtz, J.H.; Asher, S.A. Polymerized colloidal crystal hydrogel films as intelligent chemical sensing materials. *Nature* **1997**, *389*, 829–832. [CrossRef]

8. Alexeev, V.L.; Sharma, A.C.; Goponenko, A.V.; Das, S.; Lednev, I.K.; Wilcox, C.S.; Finegold, D.N.; Asher, S.A. High Ionic Strength Glucose-Sensing Photonic Crystal. *Anal. Chem.* **2003**, *75*, 2316–2323. [CrossRef]
9. Goenka, S.; Sant, V.; Sant, S. Graphene-based nanomaterials for drug delivery and tissue engineering. *J. Control. Release* **2014**, *173*, 75–88. [CrossRef]
10. Tiwari, J.N.; Mahesh, K.; Le, N.H.; Kemp, K.C.; Timilsina, R.; Tiwari, R.N.; Kim, K.S. Reduced graphene oxide-based hydrogels for the efficient capture of dye pollutants from aqueous solutions. *Carbon* **2013**, *56*, 173–182. [CrossRef]
11. Firestone, B.A.; Siegel, R.A. Dynamic pH-dependent swelling properties of a hydrophobic polyelectrolyte gel. *Polym. Commun. Guildf.* **1988**, *29*, 204–208.
12. Brannon-Peppas, L.; Peppas, N.A. Dynamics and equilibrium swelling behaviour of pH-sensitive hydrogels containing 2-hydroxy methacrylate. *Biomaterials* **1990**, *11*, 635–644. [CrossRef]
13. Deen, G.R.; Mah, C.H. Influence of external stimuli on the network properties of cationic poly(*N*-acryloyl-*N*′-propyl piperazine) hydrogels. *Polymer* **2016**, *89*, 55–68. [CrossRef]
14. Kim, J.H.; Lee, S.B.; Kim, S.J.; Lee, Y.M. Rapid temperature/pH response of porous alginate-g-poly(N-isopropylacrylamide) hydrogels. *Polymer* **2002**, *43*, 7549–7558. [CrossRef]
15. Lue, S.J.; Chen, C.H.; Shih, C.M. Tuning of Lower Critical Solution Temperature (LCST) of Poly(N-Isopropylacrylamide-co-Acrylic acid) Hydrogels. *J. Macromol. Sci. Part B* **2011**, *50*, 563–579. [CrossRef]
16. Tanaka, T. Collapse of gels and the critical endpoint. *Phys. Rev. Lett.* **1978**, *40*, 820–823. [CrossRef]
17. Alzari, V.; Monticelli, O.; Nuvoli, D.; Kenny, J.M.; Mariani, A. Stimuli Responsive Hydrogels Prepared by Frontal Polymerization. *Biomacromolecules* **2009**, *10*, 2672–2677. [CrossRef] [PubMed]
18. Rička, J.; Tanaka, T. Swelling of Ionic Gels: Quantitative Performance of the Donnan Theory. *Macromolecules* **1984**, *17*, 2916–2921. [CrossRef]
19. Park, T.G.; Hoffman, A.S. Sodium Chloride-Induced Phase Transition in Nonionic Poly(N-isopropylacrylamide) Gel. *Macromolecules* **1993**, *26*, 5045–5048. [CrossRef]
20. Brannon-Peppas, L.; Peppas, N.A. Time-Dependent Response of Ionic Polymer Networks to Ph and Ionic-Strength Changes. *Int. J. Pharm.* **1991**, *70*, 53–57. [CrossRef]
21. Miyata, T.; Asami, N.; Uragami, T. A reversibly antigen-responsive hydrogel. *Nature* **1999**, *399*, 766–769. [CrossRef]
22. Takashi, M.; Asami, N.; Uragami, T. Structural design of stimuli-responsive bioconjugated hydrogels that respond to a target antigen. *J. Polym. Sci. Part B Polym. Phys.* **2009**, *47*, 2144–2157, [CrossRef]
23. Miyata, T.; Asami, N.; Uragami, T. Preparation of an antigen-sensitive hydrogel using antigen-antibody bindings. *Macromolecules* **1999**, *32*, 2082–2084. [CrossRef]
24. Miyata, T.; Jige, M.; Nakaminami, T.; Uragami, T. Tumor marker-responsive behavior of gels prepared by biomolecular imprinting. *Proc. Natl. Acad. Sci. USA* **2006**, *103*, 1190–1193. [CrossRef] [PubMed]
25. Tierney, S.; Falch, B.M.H.; Hjelme, D.R.; Stokke, B.T. Determination of Glucose Levels Using a Functionalized Hydrogel Optical Fiber Biosensor: Toward Continuous Monitoring of Blood Glucose in Vivo. *Anal. Chem.* **2009**, *81*, 3630–3636. [CrossRef] [PubMed]
26. Thoniyot, P.; Tan, M.J.; Karim, A.A.; Young, D.J.; Loh, X.J. Nanoparticle–Hydrogel Composites: Concept, Design, and Applications of These Promising, Multi-Functional Materials. *Adv. Sci.* **2015**, *2*, 1400010. [CrossRef] [PubMed]
27. Gaharwar, A.K.; Peppas, N.A.; Khademhosseini, A. Nanocomposite hydrogels for biomedical applications. *Biotechnol. Bioeng.* **2014**, *111*, 441–453, [CrossRef] [PubMed]
28. Zhai, D.; Liu, B.; Shi, Y.; Pan, L.; Wang, Y.; Li, W.; Zhang, R.; Yu, G. Highly Sensitive Glucose Sensor Based on Pt Nanoparticle/Polyaniline Hydrogel Heterostructures. *ACS Nano* **2013**, *7*, 3540–3546, [CrossRef]
29. Yin, M.j.; Zhang, Y.; Yin, Z.; Zheng, Q.; Zhang, A.P. Micropatterned Elastic Gold-Nanowire/Polyacrylamide Composite Hydrogels for Wearable Pressure Sensors. *Adv. Mater. Technol.* **2018**, *3*, 1800051, [CrossRef]
30. Das, A.; Kumar, A.; Patil, N.B.; Viswanathan, C.; Ghosh, D. Preparation and characterization of silver nanoparticle loaded amorphous hydrogel of carboxymethylcellulose for infected wounds. *Carbohydr. Polym.* **2015**, *130*, 254–261. [CrossRef]
31. Liang, D.; Lu, Z.; Yang, H.; Gao, J.; Chen, R. Novel Asymmetric Wettable AgNPs/Chitosan Wound Dressing: In Vitro and In Vivo Evaluation. *ACS Appl. Mater. Interfaces* **2016**, *8*, 3958–3968. [CrossRef]

32. Tokarev, I.; Tokareva, I.; Gopishetty, V.; Katz, E.; Minko, S. Specific Biochemical-to-Optical Signal Transduction by Responsive Thin Hydrogel Films Loaded with Noble Metal Nanoparticles. *Adv. Mater.* **2010**, *22*, 1412–1416. [CrossRef] [PubMed]
33. Deen, R.G.; Chua, V. Synthesis and Properties of New "Stimuli" Responsive Nanocomposite Hydrogels Containing Silver Nanoparticles. *Gels* **2015**, *10*, 117–134. [CrossRef]
34. Politano, A.; Argurio, P.; Di Profio, G.; Sanna, V.; Cupolillo, A.; Chakraborty, S.; Arafat, H.A.; Curcio, E. Photothermal Membrane Distillation for Seawater Desalination. *Adv. Mater.* **2017**, *29*, 1603504. [CrossRef] [PubMed]
35. Politano, A.; Cupolillo, A.; Di Profio, G.; Arafat, H.A.; Chiarello, G.; Curcio, E. When plasmonics meets membrane technology. *J. Phys. Condens. Matter* **2016**, *28*, 363003. [CrossRef]
36. Politano, A.; Di Profio, G.; Fontananova, E.; Sanna, V.; Cupolillo, A.; Curcio, E. Overcoming temperature polarization in membrane distillation by thermoplasmonic effects activated by Ag nanofillers in polymeric membranes. *Desalination* **2018**. [CrossRef]
37. Calabria, U.; Politano, A.; Calabria, U.; Scaramuzza, N.; Calabria, U. Tailoring the physical properties of nanocomposite films by the insertion of graphene and metal nanoparticles. *Composites Part B* **2014**, *60*, 29–35. [CrossRef]
38. Mayer, K.M.; Hafner, J.H. Localized Surface Plasmon Resonance Sensors. *Chem. Rev.* **2011**, *111*, 3828–3857. [CrossRef]
39. Maier, S.A. *Plasmonics: Fundamentals and Applications*; Springer Science & Business Media: New York, NY, USA, 2007; pp. 1–223,
40. Klimov, V. *Nanoplasmonics*; Pan Stanford Publishing: Singapore, 2014.
41. Endo, T.; Kerman, K.; Nagatani, N.; Hiepa, H.M.; Kim, D.K.; Yonezawa, Y.; Nakano, K.; Tamiya, E. Multiple Label-Free Detection of Antigen-Antibody Reaction Using Localized Surface Plasmon Resonance-Based Core-Shell Structured Nanoparticle Layer Nanochip. *Anal. Chem.* **2006**, *78*, 6465–6475. [CrossRef]
42. Estevez, M.C.; Otte, M.A.; Sepulveda, B.; Lechuga, L.M. Trends and challenges of refractometric nanoplasmonic biosensors: A review. *Anal. Chim. Acta* **2014**, *806*, 55–73. [CrossRef]
43. Gil, E.S.; Hudson, S.M. Stimuli-reponsive polymers and their bioconjugates. *Progr. Polym. Sci.* **2004**, *29*, 1173–1222. [CrossRef]
44. Jain, P.K.; Huang, X.; El-Sayed, I.H.; El-Sayed, M.A. Noble Metals on the Nanoscale: Optical and Photothermal Properties and Some Applications in Imaging, Sensing, Biology, and Medicine. *Acc. Chem. Res.* **2008**, *41*, 1578–1586. [CrossRef] [PubMed]
45. Kelly, K.L.; Coronado, E.; Zhao, L.L.; Schatz, G.C. The optical properties of metal nanoparticles: The influence of size, shape, and dielectric environment. *J. Phys. Chem. B* **2003**, *107*, 668–677. [CrossRef]
46. Jain, P.K.; El-Sayed, M.A. Plasmonic coupling in noble metal nanostructures. *Chem. Phys. Lett.* **2010**, *487*, 153–164. [CrossRef]
47. Jain, P.K.; Eustis, S.; El-Sayed, M.A. Plasmon Coupling in Nanorod Assemblies: Optical Absorption, Discrete Dipole Approximation Simulation, and Exciton-Coupling Model. *J. Phys. Chem. B* **2006**, *110*, 18243–18253. [CrossRef] [PubMed]
48. Jain, P.K.; Huang, W.; El-Sayed, M.A. On the universal scaling behavior of the distance decay of plasmon coupling in metal nanoparticle pairs: A plasmon ruler equation. *Nano Lett.* **2007**, *7*, 2080–2088. [CrossRef]
49. Kreibig, U.; Volmerr, M. *Optical Properties of Metal Clusters*; Springer Science & Business Media: New York, NY, USA, 1995; Volume 25, p. 552.
50. Tierney, S.; Hjelme, D.R.; Stokke, B.T. Determination of Swelling of Responsive Gels with Nanometer Resolution. Fiber-Optic Based Platform for Hydrogels as Signal Transducers. *Anal. Chem.* **2008**, *80*, 5086–5093. [CrossRef]
51. Muri, H.I.; Hjelme, D.R. LSPR coupling and distribution of interparticle distances between nanoparticles in hydrogel on optical fiber end face. *Sensors* **2017**, *17*, 2723. [CrossRef]
52. Muri, H.I.D.I.H.; Bano, A.; Hjelme, D.R.D. A Single-Point , Multiparameter , Fiber Optic Sensor Based on a Combination of Interferometry and LSPR. *J. Lightw. Technol.* **2018**, *36*, 1159–1167. [CrossRef]
53. Muri, H.H.I.; Bano, A.; Hjelme, D.R.D. LSPR and Interferometric Sensor Modalities Combined Using a Double-Clad Optical Fiber. *Sensors* **2018**, *18*, 187. [CrossRef]
54. Plieva, F.M.; Karlsson, M.; Aguilar, M.R.; Gomez, D.; Mikhalovsky, S.; Galaev', I.Y. Pore structure in supermacroporous polyacrylamide based cryogels. *Soft Matter* **2005**, *1*, 303–309. [CrossRef]

55. Zhang, J.; Peppas, N.A. Morphology of poly(methacrylic acid)/poly(N-isopropyl acrylamide) interpenetrating polymeric networks. *J. Biomater. Sci. Polym. Ed.* **2002**, *13*, 511–525. [CrossRef] [PubMed]
56. Taylor, M.; Scurr, D.; Lutolf, M.; Buttery, L.; Zelzer, M.; Alexander, M. 3D chemical characterization of frozen hydrated hydrogels using ToF-SIMS with argon cluster sputter depth profiling. *Biointerphases* **2018**, *11*, 02A301. [CrossRef] [PubMed]
57. Lin, S.Y.; Chen, K.S.; Run-Chu, L. Drying methods affecting the particle sizes, phase transition, deswelling/reswelling processes and morphology of poly(N-isopropylacrylamide) microgel beads. *Polymer* **1999**, *40*, 6307–6312. [CrossRef]
58. Rüchel, R.; Brager, M.D. Scanning electron microscopic observations of polyacrylamide gels. *Anal. Biochem.* **1975**, *68*, 415–428. [CrossRef]
59. Zhang, X.Z.; Yang, Y.Y.; Chung, T.S.; Ma, K.X. Preparation and Characterization of Fast Response Macroporous Poly(N-isopropylacrylamide) Hydrogels. *Langmuir* **2001**, *17*, 6094–6099. [CrossRef]
60. Plieva, F.M.; Savina, I.N.; Deraz, S.; Andersson, J.; Galaev, I.Y.; Mattiasson, B. Characterization of supermacroporous monolithic polyacrylamide based matrices designed for chromatography of bioparticles. *J. Chromatogr. B* **2004**, *807*, 129–137. [CrossRef]
61. Savina, I.N.; Mattiasson, B.; Galaev, I.Y. Graft polymerization of acrylic acid onto macroporous polyacrylamide gel (cryogel) initiated by potassium diperiodatocuprate. *Polymer* **2005**, *46*, 9596–9603. [CrossRef]
62. Trieu, H.H.; Qutubuddin, S. Polyvinyl alcohol hydrogels I. Microscopic structure by freeze-etching and critical point drying techniques. *Colloid Polym. Sci.* **1994**, *272*, 301–309. [CrossRef]
63. Chen, J.; Park, K. Synthesis and characterization of superporous hydrogel composites. *J. Control. Release* **2000**, *65*, 73–82. [CrossRef]
64. Murali Mohan, Y.; Lee, K.; Premkumar, T.; Geckeler, K.E. Hydrogel networks as nanoreactors: A novel approach to silver nanoparticles for antibacterial applications. *Polymer* **2007**, *48*, 158–164. [CrossRef]
65. Park, S.; Murthy, P.S.K.; Park, S.; Mohan, Y.M.; Koh, W.G. Preparation of silver nanoparticle-containing semi-interpenetrating network hydrogels composed of pluronic and poly(acrylamide) with antibacterial property. *J. Ind. Eng. Chem.* **2011**, *17*, 293–297. [CrossRef]
66. Möbus, G.; Inkson, B.J. Nanoscale tomography in materials science. *Mater. Today* **2007**, *10*, 18–25. [CrossRef]
67. Kulawik, K.; Buffat, P.A.; Kruk, A.; Wusatowska-Sarnek, A.M.; Czyrska-Filemonowicz, A. Materials Characterization Imaging and characterization of γ' and γ'' nanoparticles in Inconel 718 by EDX elemental mapping and FIB-SEM tomography. *Mater. Charact.* **2015**, *100*, 74–80. [CrossRef]
68. Schneider, P.; Meier, M.; Wepf, R.; Müller, R. Serial FIB/SEM imaging for quantitative 3D assessment of the osteocyte lacuno-canalicular network. *Bone* **2018**, *49*, 304–311. [CrossRef] [PubMed]
69. Braet, F.; De Zanger, R.; Wisse, E. Drying cells for SEM, AFM and TEM by hexamethyldisilazane: A study on hepatic endothelial cells. *J. Microsc.* **1997**, *186*, 84–87. [CrossRef] [PubMed]
70. Bray, D.F.; Bagu, J.; Koegler, P. Comparison of hexamethyldisilazane (HMDS), Peldri II, and critical—Point drying methods for scanning electron microscopy of biological specimens. *Microsc. Res. Tech.* **1993**, *26*, 489–495. [CrossRef] [PubMed]
71. Perdigao, J.; Lambrechts, P.; Van Meerbeek, B.; Vanherle, G.; Lopes, A.L. Field emission SEM comparison of four postfixation drying techniques for human dentin. *J. Biomed. Mater. Res.* **1995**, *29*, 1111–1120. [CrossRef]
72. Araujo, J.C.; Téran, F.C.; Oliveira, R.A.; Nour, E.A.; Montenegro, M.A.; Campos, J.R.; Vazoller, R.F. Comparison of hexamethyldisilazane and critical point drying treatments for SEM analysis of anaerobic biofilms and granular sludge. *J. Electron Microsc.* **2003**, *52*, 429–433. [CrossRef]
73. Jusman, Y.; Ng, S.C.; Azuan, N.; Osman, A. Investigation of CPD and HMDS sample preparation techniques for cervical cells indeveloping computer aided screening system based on FE-SEM/EDX. *Sci. World J.* **2014**, *2014*, 289817. [CrossRef]
74. Annabi, N.; Mithieux, S.; Weiss, A.; Dehghani, F. The fabrication of elastin-based hydrogels using high pressure CO2. *Biomaterials* **2009**, *30*, 1–7. [CrossRef]
75. McMahon, R.; Hahn, M.; Pendleton, M.; Ellis, E. A Simple Preparation Method for Mesh Fibrin Hydrogel Composites for Conventional SEM. *Microsc. Microanal.* **2010**, *16*, 1030–1031. [CrossRef]
76. Lee, J.T.Y.; Chow, K.L. SEM sample preparation for cells on 3D scaffolds by freeze-drying and HMDS. *Scanning* **2012**, *34*, 12–25. [CrossRef] [PubMed]

77. Yoon, Y.M.; Lewis, J.S.; Carstens, M.R.; Campbell-Thompson, M.; Wasserfall, C.H.; Atkinson, M.A.; Keselowsky, B.G. A combination hydrogel microparticle-based vaccine prevents type 1 diabetes in non-obese diabetic mice. *Sci. Rep.* **2015**, *5*, 13155. [CrossRef] [PubMed]
78. Jurrus, E.; Hardy, M.; Tasdizen, T.; Fletcher, P.T.; Koshevoy, P.; Chien, C.B.; Denk, W.; Whitaker, R. Axon tracking in serial block-face scanning electron microscopy. *Med. Image Anal.* **2018**, *13*, 180–188. [CrossRef] [PubMed]
79. Denk, W.; Horstmann, H. Serial Block-Face Scanning Electron Microscopy to Reconstruct Three-Dimensional Tissue Nanostructure. *PLoS Biol.* **2004**, *2*, e329. [CrossRef]
80. Mehdizadeh Kashi, A.; Tahemanesh, K.; Chaichian, S.; Joghataei, M.T.; Moradi, F.; Tavangar, S.M.; Mousavi Najafabadi, A.S.; Lotfibakhshaiesh, N.; Pour Beyranvand, S.; Fazel Anvari-Yazdi, A.; et al. How to Prepare Biological Samples and Live Tissues for Scanning Electron Microscopy (SEM). *Galen Med. J.* **2014**, *3*, 63–80.
81. Little, B.; Wagner, P.; Ray, R.; Pope, R.; Scheetz, R. Biofilms: An ESEM evaluation of artifacts introduced during SEM preparation. *J. Ind. Microbiol.* **1991**, *8*, 213–221. [CrossRef]
82. Dolya, N.; Rojas, O.; Kosmella, S.; Tiersch, B.; Koetz, J.; Kudaibergenov, S. "One-Pot" In Situ Formation of Gold Nanoparticles within Poly(acrylamide) Hydrogels. *Macromol. Chem. Phys.* **2018**, *214*, 1114–1121. [CrossRef]
83. Goldstein, A.; Soroka, Y.; Frsšić-Zlotkin, M.; Popov, I.; Kohen, R. High resolution SEM imaging of gold nanoparticles in cells and tissues. *J. Microsc.* **2014**, *256*, 237–247. [CrossRef]
84. Bertazzo, S.; Gentleman, E.; Cloyd, K.L.; Chester, A.H.; Yacoub, M.H.; Stevens, M.M. Nano-analytical electron microscopy reveals fundamental insights into human cardiovascular tissue calcification. *Nat. Mater.* **2013**, *12*, 576–583. [CrossRef]
85. Han, D.M.; Matthew Zhang, Q.; Serpe, M.J. Poly (N-isopropylacrylamide)-co-(acrylic acid) microgel/Ag nanoparticle hybrids for the colorimetric sensing of H2O2. *Nanoscale* **2015**, *7*, 2784–2789. [CrossRef] [PubMed]
86. Bouchal, K.; Sedláková, Z.; Ilavský, M. Phase transition in swollen gels. *Polym. Bull.* **1994**, *32*, 331–338. [CrossRef]
87. Yeong, W.Y.; Chua, C.K.; Leong, K.F.; Chandrasekaran, M.; Lee, M.W. Comparison of drying methods in the fabrication of collagen scaffold via indirect rapid prototyping. *J. Biomed. Mater. Res. Part B Appl. Biomater.* **2007**, *82B*, 260–266. [CrossRef]
88. Shibayama, M.; Ikkai, F.; Inamoto, S.; Nomura, S.; Han, C.C. pH and salt concentration dependence of the microstructure of poly(*N*-isopropylacrylamide-co-acrylic acid) gels. *J. Chem. Phys.* **1996**, *105*, 4358–4366. [CrossRef]